# DNA Origami Delivery System for Cancer Therapy with Tunable Release Properties

**Yong-Xing Zhao,[†,‡] Alan Shaw,[†] Xianghui Zeng,[†] Erik Benson,[†] Andreas M. Nyström,[†] and Björn Högberg[†,*]**

[†]Swedish Medical Nanoscience Center, Department of Neuroscience, Karolinska Institute, SE-171 77 Stockholm, Sweden, and [‡]School of Pharmaceutical Sciences, Zhengzhou University, Zhengzhou 450001, Henan Province, People's Republic of China

**ABSTRACT**

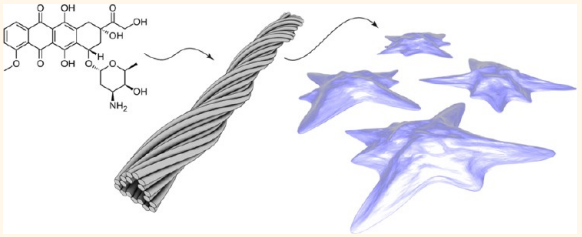

In the assembly of DNA nanostructures, the specificity of Watson–Crick base pairing is used to control matter at the nanoscale. Using this technology for drug delivery is a promising route toward the magic bullet concept, as it would allow the realization of complex assemblies that co-localize drugs, targeting ligands and other functionalities in one nanostructure. Anthracyclines' mechanism of action in cancer therapy is to intercalate DNA, and since DNA nanotechnology allows for such a high degree of customization, we hypothesized that this would allow us to tune the DNA nanostructures for optimal delivery of the anthracycline doxorubicin (Dox) to human breast cancer cells. We have tested two DNA origami nanostructures on three different breast cancer cell lines (MDA-MB-231, MDA-MB-468, and MCF-7). The different nanostructures were designed to exhibit varying degrees of global twist, leading to different amounts of relaxation in the DNA double-helix structure. By tuning the nanostructure design we are able to (i) tune the encapsulation efficiency and the release rate of the drug and (ii) increase the cytotoxicity and lower the intracellular elimination rate when compared to free Dox. Enhanced apoptosis induced by the delivery system in breast cancer cells was investigated using flow cytometry. The findings indicate that DNA origami nanostructures represent an efficient delivery system for Dox, resulting in high degrees of internalization and increased induction of programmed cell death in breast cancer cells. In addition, by designing the structures to exhibit different degrees of twist, we are able to rationally control and tailor the drug release kinetics.

**KEYWORDS:** DNA nanotechnology · cancer drug delivery · DNA origami · breast cancer cells · doxorubicin · cell uptake

In the assembly of DNA nanostructures, the specificity of Watson–Crick base pairing is used to control matter at the nanoscale.[1−7] With this technology, nanoscale assemblies of drugs, ligands, and other functionalities can be organized with unprecedented precision for targeting[8] and even to perform simple logic to deliver payloads only when needed.[8,9] This technique will allow researchers to move closer to the goal of building the magic bullet for cancer, a concept introduced by Paul Erhlich in the 20th century. Compared to many other nanoscale systems designed for drug delivery such as polymer micelles and inorganic particles, DNA origami based construction has several advantages: (i) same size, shape, and charge for each particle instead of the size distribution often seen for self-assembled nanostructures; (ii) perfect control of the placement of functionalities on the structure using specific oligos. The above features suggest that these nanostructures should be considered a promising tool for cancer nanotechnology[10] in the future. So far, DNA origami nanostructures have been used to successfully deliver different cargos to cells, such as immunostimulatory oligonucleotides[11] or apoptosis-inducing antibodies.[8] Anthracyclines for cancer therapy[12] intercalate DNA,[13,14] and since DNA nanotechnology allows such a high degree of customization, the question is whether it is possible to tune the DNA nanostructures to optimize the delivery of doxorubicin (Dox) to human cancer cells. Recently Ke *et al.*[15] demonstrated that by designing DNA origami nanostructures to have a certain twist density, the structures would fold correctly only when a certain amount of intercalator was added to the folding reaction. Here, we investigate whether such an alternation in the origami design would enable a change in the drug loading and release properties. To analyze how the *in vitro* drug kinetics correspond to changes in cellular delivery, we also investigate how the different designs affect the viability of three common breast cancer cell lines: MDA-MB-231, MDA-MB-468, and MCF-7.

Received for review May 22, 2012 and accepted September 5, 2012.

**Published online September 05, 2012**
10.1021/nn3022662

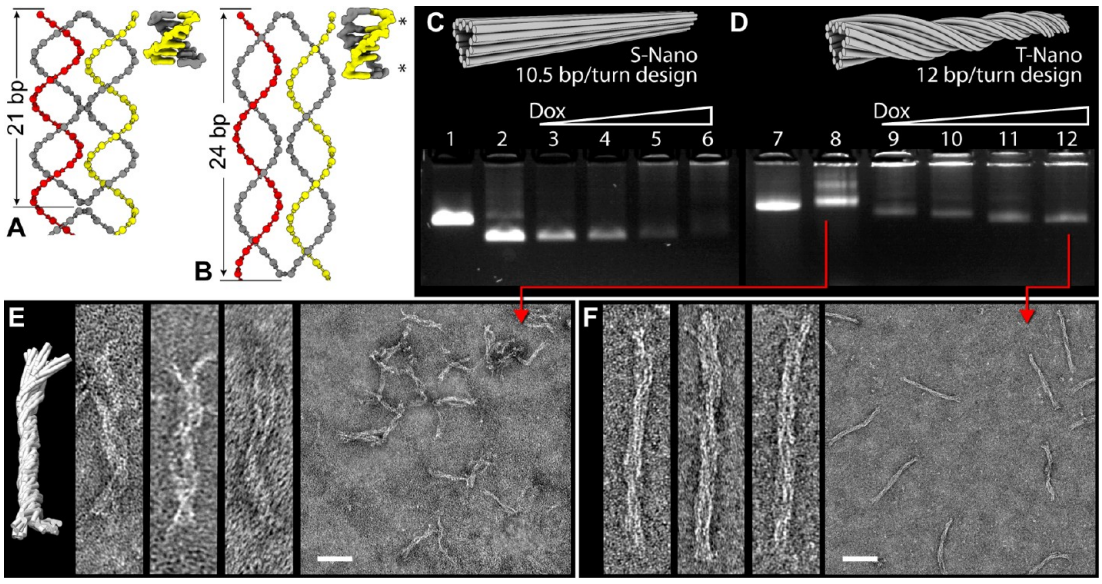


**Figure 1. Nanostructure design and characterization. (A and B) Dox intercalation shifts the pitch and twist density of DNA. Crystal structure data of six base pairs of DNA without, A (from ref 17), and with Dox, B (from ref 18), intercalation at the sites marked with * (to scale, rendered with Molecular Maya[29] from PDB structures). Ball-and-stick simplified DNA models of 24 base pairs are shown in the same scale. Without Dox, normal B-type DNA has a twist density of 10.5 bp per turn, leading to origami designs where 21 bp separate two consecutive crossovers. With Dox intercalation the twist density appears to shift to 12 bp per turn, and origami designs where 24 bp separate two consecutive twists would constitute a relaxed design. (C) Straight nanotube (S-Nano) design using 10.5bp per turn twist density. 3D model where each dsDNA helix is represented by a cylinder. 2% Agarose gel elctrophoresis showing the folding quality at different concentrations of Dox: (1) p7560 scaffold alone, (2) S-Nano no Dox, (3) S-Nano with 16 $\mu$M Dox, (4) S-Nano 32 $\mu$M Dox, (5) S-Nano 64 $\mu$M Dox, (6) S-Nano 96 $\mu$M Dox. (D) Twisted, 12bp/turn, design (T-Nano). Simple 3D model (not based on simulation) and gel data: (7) p8634 scaffold alone, (8) T-Nano no Dox, (9) T-Nano 16 $\mu$M Dox, (10) T-Nano 32 $\mu$M Dox, (11) T-Nano 64 $\mu$M Dox, (12) T-Nano 96 $\mu$M Dox. (E) CanDo prediction[30] and TEM micrographs of T-Nano folded without Dox. (F) TEM micrographs of T-Nano folded with 96 $\mu$M Dox. In both E and F: 50 $\times$ 200 nm close-ups and a 800 $\times$ 800 nm field of view, 100 nm scale bars.**

## RESULTS AND DISCUSSION

To investigate the feasibility of using DNA origami nanostructures as a drug delivery system for Dox, we designed two 18-helix bundle nanotubes using the honeycomb lattice framework[3] and using caDNAno[16] for the design work (complete design schematics and sequences in supplementary Figures S1 and S2). The first of these test structures was a straight nanotube (S-Nano) using a conventional number of 10.5 bases per helical turn of DNA to determine crossover positions between neighboring helices. The S-Nano design, depicted schematically in Figure 1C, was designed to use a 7560 nt long scaffold[3] and to be 138 nm long with a diameter of 13 nm and folds correctly in the absence of Dox; see supplementary Figure S3. Using the same S-Nano design as a starting point, a twisted version (T-Nano) was designed by adding one insertion every seventh base pair following the technique introduced by Dietz *et al.*[6] To accommodate the additional base pair requirements after adding insertions, an 8634 nt long ssDNA scaffold[3] was used in this design. By designing the structure to have 12 bp per turn, it is expected that the entire structure would adopt a global right-handed twist to partially relieve the stress induced by imposing an unnatural twist density on the DNA. Indeed, we find that structure predictions and TEM data show an extremely twisted shape when this structure is folded in the absence of Dox, Figure 1E. When the structures are folded in the presence of Dox, the S-Nano, designed for 10.5 bp per turn, exhibits decreased folding quality, as can be observed by lower gel mobility (Figure 1C). Conversely, the T-Nano, designed to have 12 bp/turn, exhibits a higher yield and an increased folding quality when Dox is added; see Figure 1D. Further, TEM data of the T-Nano structures loaded with Dox (Dox/T-Nano), in Figure 1F, show that these structures are more compact, straighter, and more elongated with a general appearance of superior folding quality than the T-Nano folded without Dox in Figure 1E. This observation can be understood by examining known crystal structures of DNA. In Figure 1A and B, we show crystallography data for six base pairs of DNA from normal DNA[17] and DNA intercalated with Dox.[18] By plotting these data together with a simplified DNA model on the same scale, it becomes apparent that a more elongated DNA with a 12 bp/turn twist density should become the dominant structure after Dox intercalation. The gel data presented are captured after spin filtration to remove excess staple oligonucleotides; see Materials and Methods.

Next, we proceeded to examine whether the twist design was able to encapsulate and retain Dox at a higher rate, *via* measurements of the *in vitro* drug

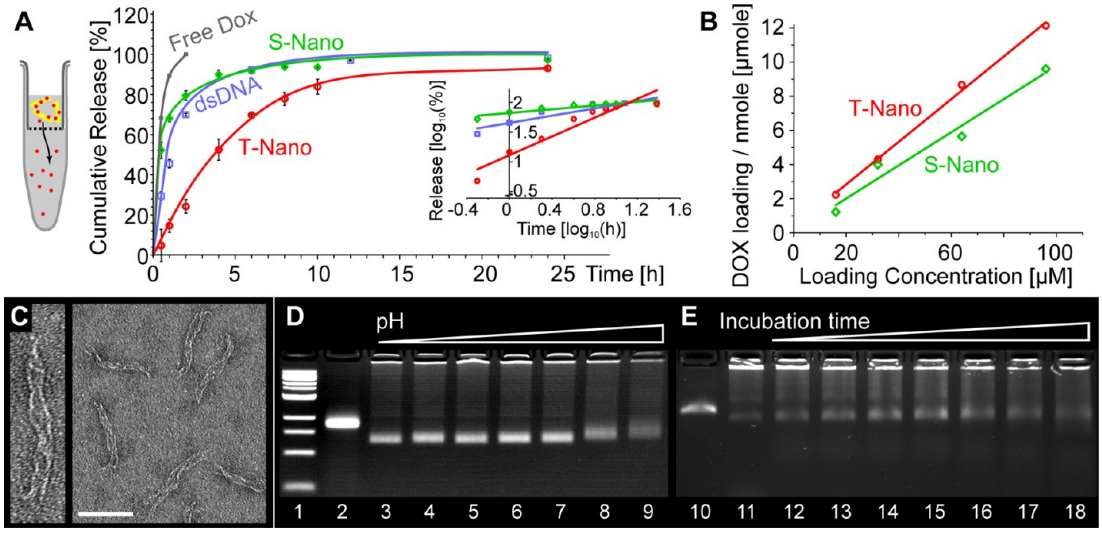


**Figure 2. DNA nanostructures as a drug delivery carrier. (A) The release rates of the different carriers were measured by measuring the fluorescence intensity of Dox after diffusion through a dialysis membrane permeable only to small molecules. Linear plot where the release curve of free Dox is shown as a reference baseline. Inset: log−log plot of the same release data with a linear regression fit. S-Nano: green; dsDNA: blue; and T-Nano: red. (B) Loading capacity of the T-Nano *vs* the S-Nano structures with linear regression. The concentration on the *x*-axis is used to equilibrate the structures with Dox. Immediately after washing away the excess Dox, the amount of Dox bound to the nanostructures is measured and plotted on the *y*-axis. (C) TEM micrographs of T-Nano folded in 96 $\mu$M Dox after *in vitro* release for 24 h. 50 × 200 nm close-up and 350 × 350 nm overview with 100 nm scale bar. (D) 2% agarose gel electrophoresis image showing the stability of the Dox-loaded T-Nano in various pH buffers for 30 min: (1) 1 kb ladder, (2) p8634 scaffold alone, Dox/T-Nano in (3) pH 4.0, (4) pH 5.0, (5) pH 6.0, (6) pH 7.0, (7) pH 7.8, (8) pH 9.0, (9) pH 10. (E) 2% agarose gel showing the T-Nano (no Dox) stability in cell culture medium with 10% fetal bovine serum: (10) p8634 scaffold alone, (11) T-Nano not incubated, (12) 30 min incubation, (13) 1 h, (14) 3 h, (15) 6 h, (16) 12 h, (17) 24 h, (18) 48 h incubation.**

release properties of the different nanotubes. As an additional control, a normal double-stranded DNA sample (dsDNA) was also used to verify if the nanostructured DNA exhibited any different properties than just plain double-stranded DNA, previously suggested as a carrier for Dox.[19,20] For this experiment a sample of M13mp18 RF DNA was used as a negative control since the sequence of this DNA to a large extent is the same as the sequence in the different scaffold DNA samples used. The *in vitro* release rate of Dox from the structures was studied by measuring the Dox fluorescence at the other side of a semipermeable membrane (see schematic in Figure 2A). One can see large differences in the release kinetics when comparing the T-Nano design with the S-Nano design. The T-Nano design manages to retain the drug to a greater extent and exhibits a slower release profile. Importantly, 50% of the Dox still remains bound to the T-Nano after several hours. In contrast, the straight, S-Nano design shows little or no significant difference in drug retention when compared to a simple, nonstructured dsDNA sample. The inset in Figure 2A shows the release data plotted in a log−log diagram. After analyzing the data using the Higuchi model[21] and the Korsmeyer−Peppas model,[22] the $r^2$ values of the Higuchi fit were found to be less than 0.9 (corresponding plot can be found in supplementary Figure S6), and the best fit for the various DNA samples could be obtained using Korsmeyer−Peppas' model for kinetic release. In this model the fraction of released drug is exponential with respect to time and the release time-exponent is dependent on the type of diffusion displayed by the material. From the log−log plot we find that the slopes of the release curves are 0.16, 0.31, and 0.79 for the Dox/S-Nano, Dox/dsDNA, and Dox/T-Nano, respectively, indicating that the Dox/dsDNA and Dox/S-Nano tended to exhibit Fickian diffusion characteristics, whereas the Dox/T-Nano indicated a non-Fickian release behavior.[23]

The loading capacity, or encapsulation efficiency, of the two types of nanostructured DNA was also measured and are presented in Figure 2B. We observe that the T-Nano is able to encapsulate significantly more Dox per structure compared to the S-Nano. The difference in loading capacity is 33% higher for T-Nano at a 96 $\mu$M loading concentration compared to S-Nano. This increase can only partially be explained by the fact that T-Nano contains 14% more base pairs per structure, but apart from that, the increased loading capacity is probably an effect of a higher affinity for Dox in the 12bp/turn design due to the relaxation of the structure as Dox is intercalated (see Figure 1).

After *in vitro* release for 24 h, the T-Nano structures look very similar (see Figure 2C) to the structures folded without Dox (Figure 1E). Moreover, gel analysis of the Dox/T-Nano complexes strongly suggests that the structures are stable in the pH range used in the cell-based assays (Figure 2D). By looking at the stability of the T-Nano without loaded Dox in a gel shift assay, it was

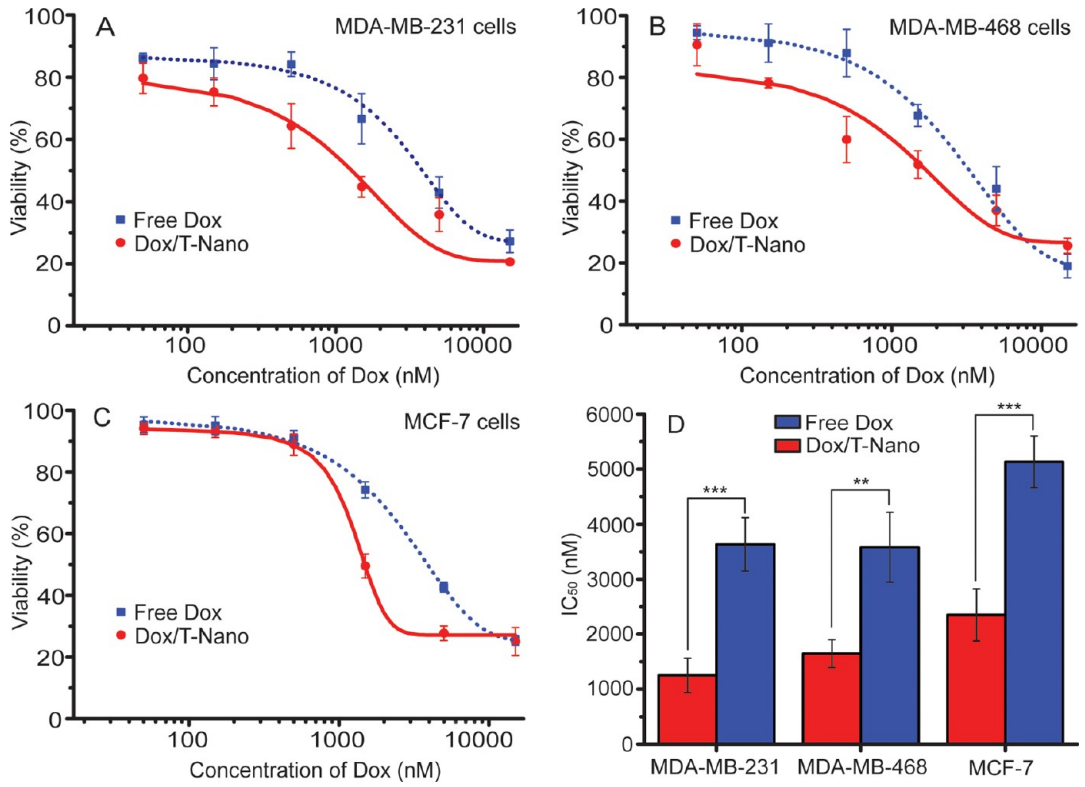


**Figure 3. Cytotoxicity of free Dox and Dox/T-Nano against MDA-MB-231 cells (A), MDA-MB-468 cells (B), and MCF-7 cells (C) after 48 h incubation. The half-maximal inhibitory concentration, $IC_{50}$, values (D) were calculated by GraphPad Prism using nonlinear regression analysis. The sulforhodamine B (SRB) assay suggested that Dox/T-Nano was more cytotoxic than free Dox to breast cancer cells. *t* test: ***$p < 0.001$, **$p < 0.01$ when compared to free Dox. Data represent mean ± SD ($n = 4$).**

possible to rule out gel shift and the implied structural change attributable to Dox release. The T-Nano structure seems to be stable over the time spans used in this report; see Figure 2E (see supplementary Figure S7 for a gel of Dox-loaded T-Nano over the same time span). Interestingly, the S-Nano structure appears not to reversibly return to its ground state after 24 h release as T-Nano does; see supplementary Figure S3 for additional TEM images and agarose gels of the structures at various stages after release of Dox.

Similarly to most controlled release systems[24] and as verified by our release rate mesurements, Dox will start to diffuse out of the nanostructures immediately upon transfer to an environment with a low Dox concentration, such as the cell culture. But because of the retention capabilities of the T-Nano, the Dox is released primarily at the cells due to cell binding and uptake of the nanostructures. The current opinion is that DNA structures get degraded after endocytosis followed by the release of Dox inside endocytotic vesicles.[14] Our data, although not sufficient to directly support this effect, are consistent with such an interpretation.

The cytotoxicity of Dox/T-Nano was examined by the sulforhodamine B colorimetric assay (SRB).[25] Three breast cancer cell lines were examined: MDA-MB-231, MDA-MB-468, and MCF-7. The cell viability was measured after 48 h incubations with drug or drug-loaded nanostructures. As can be seen in Figure 3, the half-maximal inhibitory concentration, $IC_{50}$, of Dox is significantly lower when delivered encapsulated in T-Nano structures than when added as free Dox. This fact, together with the relatively slow release profile of the T-Nano, is encouraging, as it constitutes a solid foundation for the continued development of a nanostructure-based targeted delivery system for cancer therapy. It should be noted that the Dox/S-Nano and Dox/dsDNA showed higher $IC_{50}$ values in the cases where these could be compared with Dox/T-Nano (see supplementary Figure S4 B). Since these systems also exhibited faster release profiles and less loading (Figure 2A and B), we maintain that a Dox/DNA nanostructure delivery system not using underwinding like in T-Nano is no more efficient than a system based on simple double-stranded plasmid DNA. Empty nanotubes without Dox were nontoxic (data shown in supplementary Figure S4 A).

Confocal microscopy was performed to investigate cellular uptake of the Dox/T-Nano system. To follow the nanostructures, one of the staple oligonucleotides was labeled with Alexa 488. Since DAPI binds to DNA, and would thus stain our nanostructures,

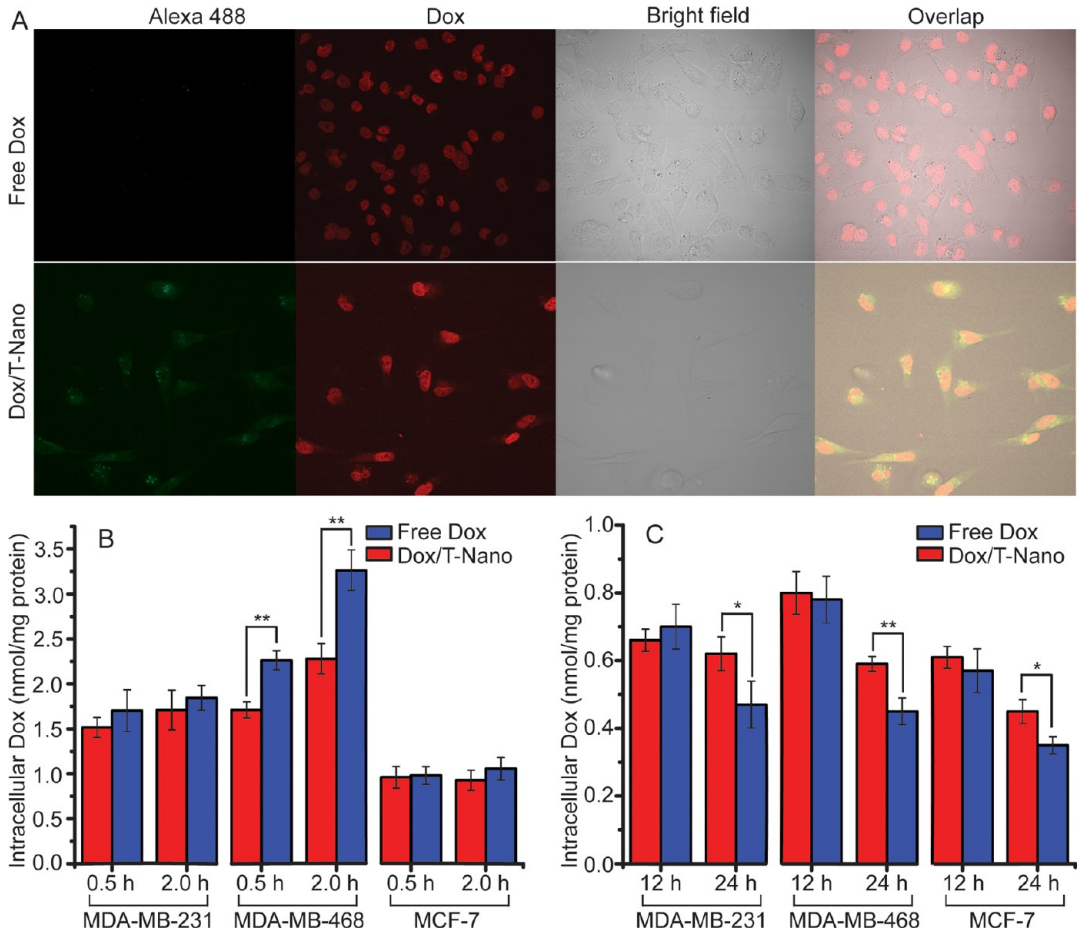


**Figure 4. Internalization and intracellular Dox level after incubation with free Dox and Dox/T-Nano. (A) Confocal microscopy images of monolayer MDA-MB-231 cells exposed to free Dox and Dox-loaded Alexa 488-labeled twisted nanotubes for 2 h. Confocal images certified that Dox could be delivered to the nucleus through Dox/T-Nano. (B) Intracellular Dox level in MDA-MB-231 cells, MDA-MB-468 cells, and MCF-7 cells exposed to free Dox and Dox/T-Nano for 0.5 and 2 h. (C) Elimination of intracellular Dox. MDA-MB-231 cells, MDA-MB-468 cells, and MCF-7 cells were incubated with free Dox and Dox/T-Nano for 2 h and then continued to be cultured in fresh medium (absent Dox). The Dox level was determined at 12 and 24 h. The concentration of Dox (free or equivalent) in cell culture was 5 $\mu$M in all the experiments. *t* test: $^{**}p < 0.01$, $^{*}p < 0.05$ when compared with free Dox. Data represent mean ± SD ($n = 3$).**

we decided not to use DAPI for nuclear staining after verifying this fact. Results from the confocal imaging can be found in Figure 4A, and the Alexa 488-labeled T-Nano is clearly taken up by the cells. Moreover, the Dox/T-Nano seems to efficiently deliver Dox to the cell nuclei.

Similarly to earlier studies of DNA nanostructure uptake by cells,[11,26,27] only one of the components was labeled (in this case, one staple with Alexa 488), so similarly to these reports, the data do not exclude a scenario where the structures would be bound to the surface, degraded, or otherwise destabilized followed by uptake of some of the components. Nevertheless, the data are also consistent with the hypothesis that large (≥7kb) DNA nanostructures are completely endocytosed by mammalian cells,[11] and our opinion is that this is the most likely scenario.

To quantitatively investigate the uptake of Dox in the case of free drug or bound in Dox/T-Nano, living cells in culture were examined by measuring the Dox fluorescence intensity after incubation for 0.5 or 2 h (see Figure 4B). After these relatively short incubation times, the levels of intracellular Dox appear to be higher in the case of free drug than when delivered in T-Nano. However, if excess Dox/T-Nano or free Dox is washed away after 2 h, the intracellular levels of Dox are significantly higher in the case of Dox/T-Nano after continued growth in fresh culture medium for 12 or 24 h (see Figure 4C). This series of observations indicate that the cellular elimination is lower for Dox bound to T-Nano compared to the free drug. Our interpretation of the results is that free Dox as well as Dox/T-Nano is endocytosed as discussed above, followed by diffusion of the small Dox molecules from the endosomes to the cytosol and finally to the nucleus. The difference in depletion rates for the free drug and Dox/T-Nano can most likely be attributed to an intracellular depot effect. Here we hypothesize that the DNA nanostructures are slowly degraded in the endosomes and the Dox gets released over an

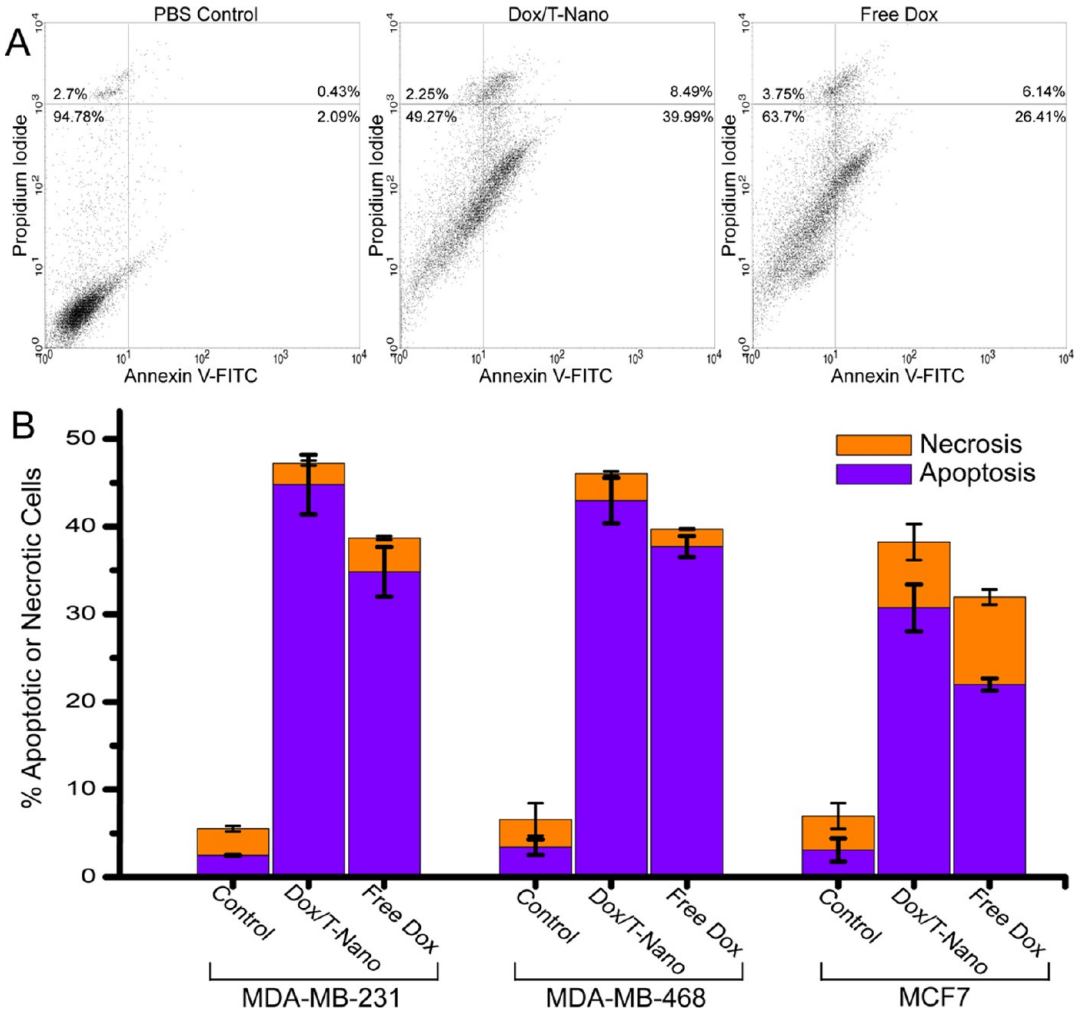


**Figure 5. Evaluation of the mechanisms of breast cancer cells treated with PBS (control), free Dox, and Dox/T-Nano. (A) Representative dot plots showing fluorescence channel analyses of MDA-MB-468 cells after dual staining with FITC-conjugated annexin V and propidium iodide. The cells were treated with free Dox and Dox/T-Nano for 48 h and stained with FITC-conjugated annexin V (green fluorescence, horizontal axis) and propidium iodide (red fluorescence, vertical axis) before being analyzed using flow cytometry and fluorescence-activated cell sorting protocols. FITC-conjugated annexin V binding to phosphatidylserine in the absence of propidium iodide staining is indicative of early apoptosis. (B) Comparison of cell apoptosis rate of MDA-MB-231 cells, MDA-MB-468 cells, and MCF-7 cells exposed to free Dox and Dox/T-Nano for 48 h. Dox/T-Nano induced significant apoptosis compared with free Dox. The concentration of Dox (free or equivalent) in cell culture was 10 $\mu$M in all experiments. Data represent mean $\pm$ SD ($n$ = 3).**

extended period of time, with the endosomes acting as local depots. In contrast, free Dox would get transported in quickly, but reversely it would also diffuse out of the cells at a higher rate. This is, however, speculative. The details of DNA-nanostructures uptake in cell culture remain to a large extent unknown, and further microscopy studies are needed to elucidate the exact pathway.

Induction of apoptosis is the desired mechanism for Dox-mediated anticancer therapy. To investigate whether this system merely caused more necrosis or indeed enhanced the inherent properties of Dox, the apoptotic effects of the T-Nano were investigated by fluorescence activated cell sorting. Using a combination of FITC-labeled annexin V[28] and propidium iodide, cells were sorted into populations of live, necrotic, and apoptotic cells. The main results for free Dox and Dox/T-Nano are summarized in Figure 5. Whereas necrosis remains more or less widespread across the negative control (PBS buffer), Dox/T-Nano, and free Dox, a considerable increase in apoptotic cells was observed for Dox/T-Nano compared to free Dox.

## CONCLUSIONS

These findings indicate that DNA origami nanostructure represents an efficient delivery system for Dox internalization to induce apoptosis in breast cancer cells at lower concentrations than what is needed for free Dox. In addition, by designing the structures to exhibit different amounts of twist, we are able to rationally control and tailor the drug release kinetics. We find that by using conventional, straight DNA nanostructures the cytotoxicity and release kinetics are comparable to those obtained by using simple plasmid

DNA. In contrast, by using a twisted 12bp/turn design, a system with superior drug delivery characteristics is achieved. The promising release kinetics and cytotoxicity of the Dox/T-Nano system, in combination with the well-known flexibility of the DNA origami method to decorate the structures with targeting ligands,[10] make this a promising candidate platform for active targeting of nanostructures intended for anticancer therapy.

## MATERIALS AND METHODS

**Folding of DNA Origami Nanostructures.** Each sample was prepared by combining a 5 nM scaffold (p7560 or p8634, derived from M13mp18), 25 nM of each staple oligonucleotide, buffer, and salts including 5 mM Tris, 1 mM EDTA (pH 7.8 at 20 °C), and 10 mM $MgCl_2$. Folding was carried out by rapid heat denaturation followed by slow cooling from 80 to 60 °C over 80 min, then 60 to 24 °C over 173 h. To remove the excess staples and/or free doxorubicin, the DNA nanostructure suspensions were added to VIVAspin 500 (molecular cutoff of 100 kD, Sartorius Stedim Biotech GmbH) and centrifuged at 3000*g* for 30 min followed by suspension in Tris buffer (5 mM Tris, 1 mM EDTA, and 13 mM $MgCl_2$). Samples were electrophoresed on 2% agarose gels (0.5× TBE, 11 mM $MgCl_2$, 0.5 $\mu$g/mL ethidium bromide) at 70 V for 3 h in an ice−water bath.

**Electron Microscopy.** A 3 $\mu$L aliquot of Dox/T-NanoT sample was spotted on a glow-discharged, carbon-coated Formvar grid (Electron Microscopy Sciences), incubated for 20 s, blotted off with filter paper, and then stained with 2% (w/v) aqueous uranyl formate solution. EM analysis was performed using a FEI Morgagni 268(D) transmission electron microscope at 80 kV with nominal magnifications between 12 000 and 44 000. Images were recorded digitally by using the Advanced Microscopy Techniques Image Capture Engine 5.42.

**Stability of Doxorubicin-Intercalated Nanotube.** The Dox-intercalated nanotube was incubated with culture medium (including 10% fetal bovine serum) at 37 °C for 30 min, 1, 3, 6, 12, 24 and 48 h or in various pH (4.0, 5.0, 6.0, 7.0, 7.8, 9.0, and 10.0) Tris buffer (5 mM Tris, 1 mM EDTA) for 30 min, and then the stability was verified using agarose (2%) gel electrophoresis (0.5× TBE, 11 mM $MgCl_2$, 0.5 $\mu$g/mL ethidium bromide) at 70 V for 3 h in an ice−water bath.

**Drug Intercalation Efficiency.** To determine Dox intercalaction efficiency, 60 $\mu$L of Dox-intercalated nanotube was added into VIVaspin 500 (molecular cutoff of 100 kD, Biotech) and centrifuged at 3000*g* for 30 min. Dox content in the filtrate as free drug was measured using a microplate reader. The drug intercalaction efficiency (%) was calculated by the following equation: Intercalaction efficiency (%) = $(D_{total} - D_{free})/D_{total} \times 100$. $D_{total}$ is the Dox content in Dox-intercalated nanotube solution; $D_{free}$ is the Dox content in the filtrate.

***In Vitro* Drug Release Behaviors of Doxorubicin-Intercalated Nanotube.** The dialysis units with molecular weight cutoff of 20 000 Da were used to carry out the drug release experiments. Phosphate-buffered saline (PBS, pH = 7.4) was used as the drug release media. The sample Dox-intercalated nanotube or Dox solution (30 $\mu$L) was put into the dialysis unit. The sealed dialysis units were put into a polystyrene flotation device, floating on a surface of 1000 mL of release media in a beaker. The release medium was stirred at a speed of 200 rpm at 37 °C protected from light. At certain time intervals, the dialysis unit was taken out and 10 $\mu$L of Dox-intercalated nanotube was taken out from the dialysis unit for measuring the nonreleased drug concentrations by the microplate reader.

***In Vitro* Cytotoxicity Assay.** The cytotoxicity of empty nanotubes, free Dox, Dox/S-Nano, Dox/T-Nano, and Dox/dsDNA was tested against breast cancer cell lines MCF-7, MDA-MB-231, and MDA-MB-468 (MCF-7 human breast adenocarcinoma cell line ER pos., 231 adenocarcinoma ER neg., 468 adenocarcinoma ER neg.). The cells were obtained from ATCC (American Tissue Culture Collection, Manassas, VA, USA) and maintained according to instructions. The cytotoxicity was evaluated by the sulforhodamine B cell cytotoxicity assay (G-Biosciences, St Louis, MO, USA). Cells were cultured in Dulbecco's modified Eagle medium supplemented with 10% fetal bovine serum, 100 units/mL penicillin, and 100 mg/mL streptomycin under 5% $CO_2$ at 37 °C and collected by trypsinization using 0.25% trypsin solution. Cells were seeded in 96-well plates (Costa, Corning Incorporated) at a density of $1 \times 10^4$ cells/well and incubated for 24 h to allow for cell attachment. The cells were incubated with Dox/T-Nano or Dox at equivalent drug concentrations ranging from 50 to 15 000 nM for 48 h. At the end of the experiment, the SRB assay was performed according to the manufacturer's instructions. The absorbance was measured at 565 nm using a microplate reader. Cell viability rate was calculated by the following equation:

$$\text{Cell viability rate } (\%) = (A_{drug} - A_{blank})/(A_{control} - A_{blank}) \times 100$$

$A_{drug}$ is the absorbance of the cells incubated with Dox/T-Nano or Dox; $A_{control}$ is the absorbance of the cells incubated with the culture medium only; and $A_{blank}$ is the absorbance of the culture medium.

**Intracellular Uptake of Doxorubicin-Intercalated Twisted Nanotube.** For the Dox/T-Nano uptake study, 12-well plates were seeded with breast cancer cells at $2 \times 10^5$ per well, and the cells were allowed to attach for 24 h. The medium was replaced with 1 mL of medium containing Dox/T-Nano or Dox solution (final Dox concentration 5 $\mu$M) and incubated for 0.5 and 2 h. Cells were washed three times to remove the free Dox/T-Nano or Dox with PBS buffer and lysed in 100 $\mu$L of cell lysis buffer for 10 min. A 10 $\mu$L amount of cell lysate was used to quantitate protein concentration by the BCA assay. The remaining portion was extracted by dissolving each sample in 0.2 mL of acidified methanol (0.1 M HCL, 90% methanol) solution, and the supernatant was analyzed for Dox level using the microplate reader (excitation wavelength: 485 nm, emission wavelength: 591 nm) after centrifugation at 16800*g* for 10 min. The data were normalized to per milligram cell protein.

**Intracellular Elimination of Doxorubicin.** For the Dox/T-Nano elimination study, 12-well plates were seeded with breast cancer cells at $2 \times 10^5$ per well, and the cells were allowed to attach for 24 h. The medium was replaced with 1 mL of medium containing Dox/T-Nano or Dox solution (final Dox concentration 5 $\mu$M) and incubated for 2 h. Cells were washed three times to remove the free Dox or Dox/T-Nano with PBS buffer and continued to incubate with fresh medium. Intracellular Dox level was determined at 12 and 24 h using the same method as that described above for intracellular uptake assay.

**Internalization of Doxorubicin-Intercalated Twisted Nanotube.** Confocal laser scanning microscopy (CLSM, Olympus FV1000) further confirmed the cellular uptake of Dox/T-Nano. MDA-MB-231 cells were plated at a density of $1 \times 10^5$ cells/well containing 22 mm sterile coverslips for 24 h. Dox and the Dox/T-Nano with equivalent Dox concentration (5 $\mu$M) were incubated for 2 h, and then the cells were washed three times with PBS and fixed with 3.7% formaldehyde in PBS. Vectashield (Vector Laboratories, Inc. Burlingame, CA, USA) was dropped on the slides to seal the cell samples after the cells were washed three times with PBS. The stained coverslips were imaged using CLSM.

**Cell Apoptosis Analysis.** Apoptotic cells were determined by dual staining with an annexin V-FITC and propidium iodide kit (Invitrogen, CA, USA) according to the manufacturer's instructions. In brief, the breast cancer cells were seeded into six-well culture plates at a concentration of $1 \times 10^6$ cells/well and incubated for 24 h to allow cell attachment. The cells were pretreated with Dox, Dox/T-Nano at equivalent drug concentrations (10 $\mu$M), or empty nanotubes for 48 h and collected by trypsinization using a 0.125% trypsin solution. After that, the cells were washed twice with PBS (pH = 7.4) and resuspended in 100 $\mu$L of binding buffer at a density of $1 \times 10^5$/mL. Then 2 $\mu$L of

annexin V-FITC was added, and cells were incubated at room temperature for 20 min in darkness. Then 5 $\mu$L of propidium iodide stock solution (100 $\mu$g/mL) was added after adding 400 $\mu$L of PBS, and cells were incubated for another 5 min in darkness. The cells were analyzed by flow cytometry (Becton Dickinson, Sunnyvale, CA, USA) with CellQuest software within 1 h. The numbers of cells undergoing necrosis (positive for propidium iodide), early apoptosis (positive for annexin V), and late apoptosis (double-positive for annexin V and propidium iodide) stages of apoptosis were quantified using flow cytometry.

**Statistical Analysis.** All data were expressed as mean ± SD. $IC_{50}$ values were calculated by GraphPad Prism using nonlinear regression analysis. The statistical significance was determined using a *t* test. A *p* value less than 0.05 (*i.e.*, $p < 0.05$) was considered to indicate statistical significance for all comparisons.

*Conflict of Interest:* The authors declare no competing financial interest.

*Supporting Information Available:* Structure designs, DNA sequences, additional TEM images, cytotoxicity data, and flow cytometry data are available free of charge *via* the Internet at http://pubs.acs.org.

*Acknowledgment.* The project was funded by the Swedish Research Council (VR) through a repatriation grant and a project grant to B.H. (grants 2010-6296 and 2010-5060). B.H. and A.M.N. are recipients of assistant professorships with startup funding funded by Carl Bennet AB, Karolinska Institutet, and Vinnova. A. S. is partially funded by a Karolinska Institutet faculty grant (KID). Funding support to A.M.N. by the Royal Swedish Academy of Sciences, Falk Foundation, Jeanssons Foundation, Axel and Eva Wallströms Foundation, and the Swedish Research Council (VR) under grants 2011-3720 and 2009-3259 is acknowledged. Y.X.Z. is funded by the China Scholarship Council (CSC). We acknowledge Klas Udekwu and Ana Teixeira for helpful discussions and Xiaoyuan Ren for helping Y.X.Z. get started.

## REFERENCES AND NOTES

1. Seeman, N. C. Nucleic-Acid Junctions and Lattices. *J. Theor. Biol.* **1982**, *99*, 237–247.
2. Rothemund, P. W. K.; Papadakis, N.; Winfree, E. Algorithmic Self-Assembly of DNA Sierpinski Triangles. *PLoS Biol.* **2004**, *6*, 240–252.
3. Douglas, S. M.; Dietz, H.; Liedl, T.; Högberg, B.; Graf, F.; Shih, W. M. Self-Assembly of DNA into Nanoscale Three-Dimensional Shapes. *Nature* **2009**, *459*, 414–418.
4. Rothemund, P. W. K. Folding DNA to Create Nanoscale Shapes and Patterns. *Nature* **2006**, *440*, 297–302.
5. Liedl, T.; Högberg, B.; Tytell, J.; Ingber, D. E.; Shih, W. M. Self-Assembly of Three-Dimensional Prestressed Tensegrity Structures from DNA. *Nat. Nanotechnol.* **2010**, *5*, 520–524.
6. Dietz, H.; Douglas, S. M.; Shih, W. M. Folding DNA into Twisted and Curved Nanoscale Shapes. *Science* **2009**, *325*, 725–730.
7. Högberg, B.; Liedl, T.; Shih, W. M. Folding DNA Origami from a Double-Stranded Source of Scaffold. *J. Am. Chem. Soc.* **2009**, *131*, 9154–55.
8. Douglas, S. M.; Bachelet, I.; Church, G. M. A Logic-Gated Nanorobot for Targeted Transport of Molecular Payloads. *Science* **2012**, *335*, 831–834.
9. Andersen, E. S.; Dong, M.; Nielsen, M. M.; Jahn, K.; Subramani, R.; Mamdouh, W.; Golas, M. M.; Sander, B.; Stark, H.; Oliveira, C. L. P.; *et al.* Self-Assembly of a Nanoscale DNA Box with a Controllable Lid. *Nature* **2009**, *459*, 73–76.
10. Peer, D.; Karp, J. M.; Hong, S.; Farokhzad, O. C.; Margalit, R.; Langer, R. Nanocarriers as an Emerging Platform for Cancer Therapy. *Nat. Nanotechnol.* **2007**, *2*, 751–760.
11. Schüller, V. J.; Heidegger, S.; Sandholzer, N.; Nickels, P. C.; Suhartha, N. A.; Endres, S.; Bourquin, C.; Liedl, T. Cellular Immunostimulation by CpG-Sequence-Coated DNA Origami Structures. *ACS Nano* **2011**, *5*, 9696–9702.
12. Arora, H. C.; Jensen, M. P.; Yuan, Y.; Wu, A.; Vogt, S.; Paunesku, T.; Woloschak, G. E. Nanocarriers Enhance Doxorubicin Uptake in Drug-Resistant Ovarian Cancer Cells. *Cancer Res.* **2012**, *72*, 769–778.
13. Kellogg, G. E.; Scarsdale, J. N.; Fornari, F. A., Jr. Identification and Hydropathic Characterization of Structural Features Affecting Sequence Specificity for Doxorubicin Intercalation into DNA Double-Stranded Polynucleotides. *Nucleic Acids Res.* **1998**, *26*, 4721–4732.
14. Chang, M; Yang, C.-S.; Huang, D.-M. Aptamer-Conjugated DNA Icosahedral Nanoparticles As a Carrier of Doxorubicin for Cancer Therapy. *ACS Nano* **2011**, *8*, 6156–6163.
15. Ke, Y.; Bellot, G.; Voigt, N. V.; Fradkov, E.; Shih, W. M. Two Design Strategies for Enhancement of Multilayer–DNA-Origami Folding: Underwinding for Specific Intercalator Rescue and Staple-Break Positioning. *Chem. Sci.* **2012**, *3*, 2587–2597.
16. Douglas, S. M.; Marblestone, A. H.; Teerapittayanon, S.; Vazquez, A.; Church, G. M.; Shih, W. M. Rapid Prototyping of 3D DNA-Origami Shapes with caDNAno. *Nucleic Acids Res.* **2009**, *37*, 5001–5006.
17. Ortiz-Lombardia, M.; Gonzalez, A.; Eritja, R.; Aymami, J.; Azorin, F.; Coll, M. Crystal Structure of a DNA Holliday Junction. *Nat. Struct. Biol.* **1999**, *6*, 913–917.
18. Frederick, C. A.; Williams, L. D.; Ughetto, G.; van der Marel, G. A.; van Boom, J. H.; Rich, A.; Wang, A. H. Structural Comparison of Anticancer Drug-DNA Complexes: Adriamycin and Daunomycin. *Biochemistry* **1990**, *29*, 2538–2549.
19. Bagalkot, V.; Lee, I.-H.; Yu, M. K.; Lee, E.; Park, S.; Lee, J.-H.; Jon, S. A Combined Chemoimmunotherapy Approach Using a Plasmid-Doxorubicin Complex. *Mol. Pharmaceutics* **2009**, *6*, 1019–1028.
20. Bagalkot, V.; Farokhzad, O. C.; Langer, R.; Jon, S. An Aptamer–Doxorubicin Physical Conjugate as a Novel Targeted Drug-Delivery Platform. *Angew. Chem., Int. Ed.* **2006**, *45*, 8149–8152.
21. Higuchi, T. Mechanism of Sustained-Action Medication: Theoretical Analysis of Rate of Release of Solid Drugs Dispersed in Solid Matrices. *J. Pharm. Sci.* **1963**, *52*, 1145–1149.
22. Korsmeyer, R. W.; Gurnya, R.; Doelkera, E.; Buria, P.; Peppas, N. A. Mechanisms of Solute Release from Porous Hydrophilic Polymers. *Int. J. Pharm.* **1983**, *15*, 25–35.
23. Lin, L. Y.; Lee, N. S.; Zhu, J.; Nyström, A. M.; Pochan, D. J.; Dorshow, R. B.; Wooley, K. L. Tuning Core vs. Shell Dimensions to Adjust the Performance of Nanoscopic Containers for the Loading and Release of Doxorubicin. *J. Controlled Release* **2011**, *152*, 37–48.
24. Charrois, J. R.; Allen, T. M. Drug Release Rate Influences the Pharmacokinetics, Biodistribution, Therapeutic Activity, and Toxicity of Pegylated Liposomal Doxorubicin Formulations in Murine Breast Cancer. *Biochim. Biophys. Acta* **2004**, *1663*, 167–177.
25. Skehan, P.; Storeng, R.; Scudiero, D.; Monks, A.; McMahon, J.; Vistica, D.; Warren, T. W.; Bokesch, H.; Kenney, S.; Boyd, M. R. New Colorimetric Cytotoxicity Assay for Anticancer-Drug Screening. *J. Nat. Cancer Inst.* **1990**, *82*, 1107–1112.
26. Hamblin, G. D.; Carneiro, K. M. M.; Fakhoury, J. F.; Bujold, K. E.; Sleiman, H. F. Rolling Circle Amplification-Templated DNA Nanotubes Show Increased Stability and Cell Penetration Ability. *J. Am. Chem. Soc.* **2012**, *134*, 2888–2891.
27. Ko, S.-H.; Liu, H.; Chen, Y.; Mao, C. DNA Nanotubes as Combinatorial Vehicles for Cellular Delivery. *Biomacromolecules* **2008**, *9*, 3039–3043.
28. Koopman, G.; Reutelingsperger, C. P.; Kuijten, G. A.; Keehnen, R. M.; Pals, S. T.; van Oers, M. H. Annexin V for Flow Cytometric Detection of Phosphatidylserine Expression on B Cells Undergoing Apoptosis. *Blood* **1994**, *84*, 1415–1420.
29. www.molecularmovies.com.
30. Castro, C. E.; Kilchherr, F; Kim, D.-N.; Shiao, E. L.; Wauer, T; Wortmann, P.; Bathe, M.; Dietz, H. A Primer to Scaffolded DNA Origami. *Nat. Methods* **2011**, *8*, 221–229.